

Wear of blade spreader during powder spreading in Additive Manufacturing

Lanzhou Ge ^a, Rui Xu ^a, Wenguang Nan ^{a,b,*}

^a School of Mechanical and Power Engineering, Nanjing Tech University, Nanjing 211816, China

^b Faculty of Engineering and Physical Sciences, University of Leeds, Leeds LS2 9JT, UK

ARTICLE INFO

Keywords:

Powder spreading
Wear
Jamming
DEM

ABSTRACT

The wear of blade spreader in powder spreading process in Additive Manufacturing is explored by experiment and numerical simulation using Discrete Element Method. The results identify a new mechanism for the wear of blade spreader, i.e. transient jamming of particles. Significant wear of blade spreader could be observed when the gap between the spreader and base is less than 2 times of particle diameter D_{90} . The wear depth is more sensitive to particle interlocking than particle cohesion. Large wear depth or a long scratch could be induced by bumps or spatters on the base. The wear mainly occurs at the front bottom surface of the blade spreader. A simple method is proposed to reduce the wear of the blade spreader.

1. Introduction

As an advanced innovative technology, Additive Manufacturing (AM) now has been widely and successfully used in aerospace, new energy, biology [1,2]. Among various kinds of technology, powder-based AM has gained more attraction, due to its applicability for both metal and non-metal materials [3]. In this method, a heap with micrometre sized fine powders is spread into a very thin layer by a spreading blade or a roller, and then this spread layer is locally sintered by laser or melted by electron beam. This process is repeated until the production of the final part is finished. During this process, the spreader is found to be worn, but the underlying mechanism is still unknown. Although the wear of products made by AM has been detailed explored [4,5], there is no reliable research focusing on the wear phenomenon of the spreader used in powder-based Additive Manufacturing.

The powder spreading process in Additive Manufacturing has been widely explored by experiments and simulations using Discrete Element Method (DEM) [6–10]. For example, Haeri et al. [6] found that larger particle aspect ratios or higher translational speed of the spreader could result in a lower bed quality. Nan et al. [7] simulated the powder spreading process in Additive Manufacturing, where the physical properties of single particle were all characterised by experiment, and their results showed that the particle flow was prone to be jammed at narrow spreading gap. On the other hand, as a good alternative method, DEM has also been used to study the wear problem between bulk powder

and equipment [11–20]. For example, Zolotarevskiy et al. [11] simulated the wear during impeller-tumbler test by using DEM, and found that the edges and tip of the specimen were more likely to show significant wear. Thompson et al. [12] studied the effect of mesh discretisation in DEM simulation on the damage and wear predictions, and the results showed that the wear pattern was similar for different discretisation, but the location of the maximum wear varied. Kalácska et al. [20] simulated the soil flow during the tillage process using DEM, and found that the wear pattern of the equipment was in good agreement with the ones observed in on-site experiments. However, till now, there is no related work analysing the wear of spreader during the powder spreading process in Additive Manufacturing.

In this work, the wear of the blade spreader in powder-based Additive Manufacturing is studied, where a heap of particles is subjected to a translational motion by a vertical blade with a gap allowing a thin particle layer to be spread. The wear phenomenon of the blade spreader is observed by the experiment, and then the effects of process parameters, particle properties and the bumps of the base on the wear are investigated by numerical simulation using Discrete Element Method, followed by a simple method to reduce the wear of blade spreader. This provides a meaningful guidance for the practical application of powder spreading process in Additive Manufacturing.

* Corresponding author at: School of Mechanical and Power Engineering, Nanjing Tech University, Nanjing 211816, China.

E-mail address: nanwg@njtech.edu.cn (W. Nan).

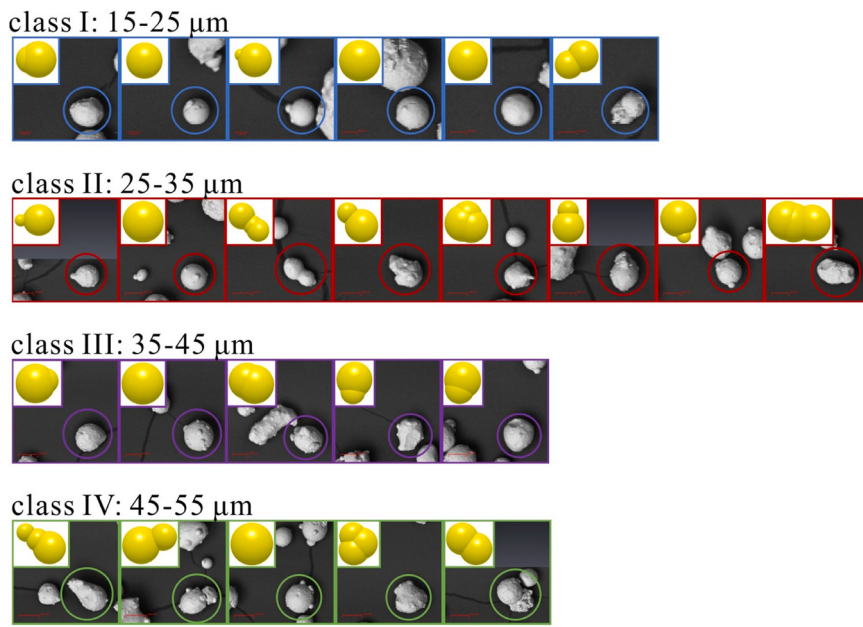


Fig. 1. Totally 24 kinds of particles used in DEM simulation [7].

2. Methods

2.1. Discrete Element Method

To describe the dynamics of powder spreading process in Additive Manufacturing, the particles are modelled as discrete entities and their motions are tracked individually by solving Newton's laws of motion [21,22], for which the Altair EDEM™ software package is used. The translational motion and rotational motion of an individual particle are given as:

$$m_i \frac{dv_i}{dt} = m_i g + \sum F_{c,i} \quad (1)$$

$$\frac{d(I_i \omega_i)}{dt} = \sum M_{c,i} \quad (2)$$

where m_i , I_i , v_i and ω_i are the mass, moment of inertia, translational velocity and angular velocity, respectively; $F_{c,i}$ is the contact force, originating from its interaction with neighbouring particles or wall; $M_{c,i}$ is the contact torque, arising from the tangential and normal contact force, as well as rolling friction resistance. In this work, the elastic contact force is described by Hertz-Mindlin contact model [22], and the adhesive interaction is accounted for by JKR theory [23], in which the normal contact force is given as:

$$F_n = \frac{4E^* a^3}{3R^*} - \sqrt{8\pi\Gamma E^* a^3} \quad (3)$$

where Γ is the interfacial surface energy; E^* is the equivalent Young's modulus; a is the contact radius, which can be calculated from the normal overlap α .

$$\alpha = \frac{a^2}{R^*} - \sqrt{\frac{2\pi\Gamma a}{E^*}} \quad (4)$$

In the unloading process, the normal contact force F_n is not zero when the normal overlap α is negative, as further work is required to separate the cohesive contact. Correspondingly, the motion resistance of particles during rolling is given as:

$$\tau_i = -\mu_r F_n R_i \omega_i \quad (5)$$

where μ_r is the coefficient of rolling friction; R_i is the distance of the contact point from particle centre, and ω_i is the unit angular velocity vector of the particle at the contact point. For simplicity, the damping force and tangential contact force are not shown here, which could be referred to Thornton [22].

2.2. Wear model

The wear of the blade spreader used in the powder spreading process is described by Archard wear model [24]. The wear volume V_w is given as:

$$V_w = K \frac{F_n \Delta U}{H_v} \quad (6)$$

where K is the wear coefficient of the material; F_n is the normal contact force; ΔU is the particle sliding distance at contact; H_v is the Vicker's hardness of the material. The wear coefficient K and hardness H_v could be related to the wear constant W in DEM simulation:

$$W = \frac{K}{H_v} \quad (7)$$

In this work, the material of 316L stainless steel is used for both particles and walls. Therefore, according to Archard's experimental data [25], the value of K is 0.007, and the corresponding value of W in the Archard wear model is 3.5×10^{-12} (1/Pa). Meanwhile, the wear depth d_w is used to describe the extent of the wear, given as:

$$d_w = \frac{V_w}{A} \quad (8)$$

where A is the area of local geometry element.

2.3. Simulation conditions

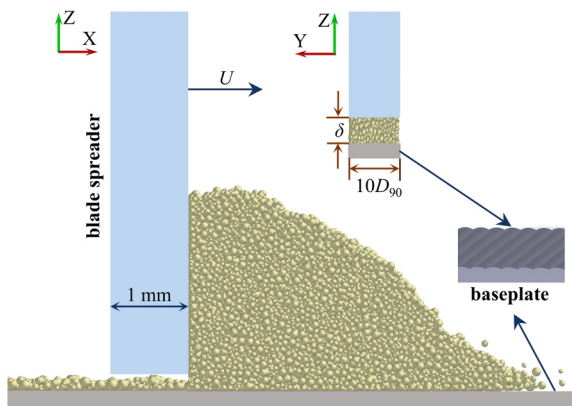
Following previous work [7], gas-atomised 316 L stainless steel particles are used, for which the number-based D_{10} , D_{50} and D_{90} are 20 μm , 32 μm and 45 μm , respectively. The particles are classified into 4 size classes, i.e. 15–25 μm , 25–35 μm , 35–45 μm and 45–55 μm . For each size class, 5–10 particles are randomly selected, with totally 24 kinds of particles being used in the DEM simulation, as shown in Fig. 1, where the non-spherical particle is described by clumped sphere

Table 1

Physical properties of single particle in the standard case [7].

Parameter	Value
Diameter, D_{90} (μm)	45
Density, ρ (kg/m^3)	7980
Young's modulus, E (GPa)	2.1
Friction coefficient*, μ_s	0.5
Restitution coefficient*, e	0.64
Interfacial surface energy*, Γ (mJ/m^2)	1.4
Rolling friction coefficient*, μ_r	0.001

* The interaction parameters of particle-wall are assumed to be the same as particle-particle.

**Fig. 2.** Set-up of the simulation system of powder spreading process.

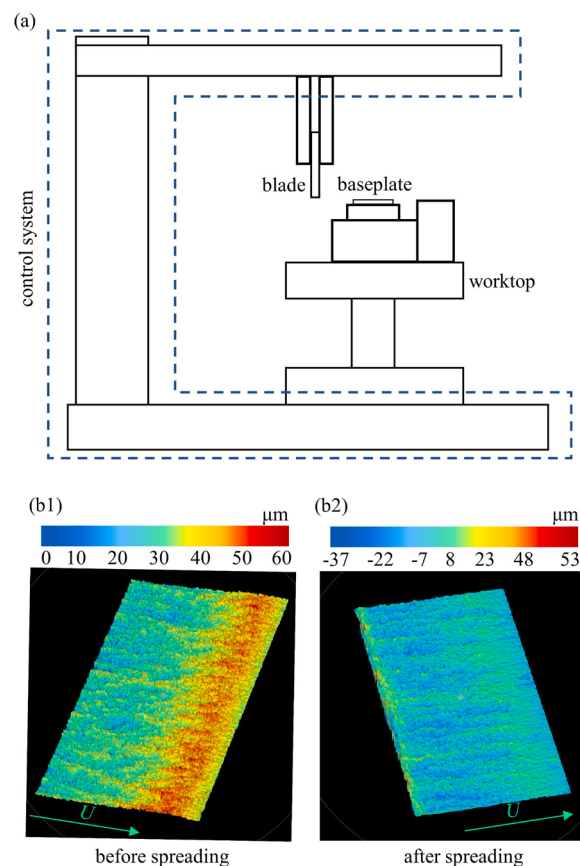
elements. The physical and mechanical properties of a single particle involved in the simulation are summarised in **Table 1**, in which the interaction parameters of particle-particle/wall are also included. These properties and parameters are all based on the experiment characterisation of single particle [7], including interfacial surface energy using drop test. It should be noted that the Young's modulus and interfacial surface energy in **Table 1** are the value after scaling, i.e. Young's modulus is scaled from $E_{exp} = 211 \text{ GPa}$ to $E_{DEM} = 2.1 \text{ GPa}$ while the interfacial surface energy is decreased from $\Gamma_{exp} = 9 \text{ mJ}/\text{m}^2$ to $\Gamma_{DEM} = 1.4 \text{ mJ}/\text{m}^2$, according to following law [26,27]:

$$\frac{\Gamma_{DEM}}{\Gamma_{exp}} = \left(\frac{E_{DEM}}{E_{exp}} \right)^{2/5} \quad (9)$$

In this way, larger time step could be used in DEM to speed up the simulation.

The simulation system consists of a spreading blade and a base, as shown in **Fig. 2**. The base is described by overlapping cylinders to provide a rough surface, and its total length and width are $400D_{90}$ and $10D_{90}$, respectively. The thickness of the blade is 1 mm. Periodic boundary conditions are applied in the Y direction of the simulation system. The materials of the blade and base are assumed to be the same as that of particles with properties shown in **Table 1**. The particles are firstly generated by the raining method, forming a heap in front of the blade. Then the blade is quickly and vertically lifted to the specified position in 0.005 s, forming a gap with height of δ above the top surface of rough base. Afterwards, the blade accelerates quickly in the spreading direction to the specified speed in 0.02 s, and then moves forward at this constant speed, while the particles are spread onto the rough base. The total simulation time is 0.2 s, and the total wear track of the blade is 14.8 mm. The time step used in the DEM simulation is $1e-8$ s.

In the powder-based Additive Manufacturing, the cohesion and shape of particles could show significant variation for different kinds of powder, and they have significant effects on the blade spreading system. Meanwhile, the base is the melted layer in previous cycle, in which the

**Fig. 3.** Wear phenomenon of the blade spreader in the experiment: (a) schematic of experimental system; (b) spectrograms of the bottom surface of the blade spreader.

defects may be induced during the sintering process, such as spatters [28–30], resulting in bumps on the surface of the base. Therefore, besides spreading conditions (i.e. gap height and spreading speed), the effects of another two kinds of factors on the wear phenomenon of blade are also explored: particle characteristics (i.e. cohesion and rolling friction of particles), and bumps on the base surface, as detailed reported in following sections. In the standard case, the spreading speed is 80 mm/s, the gap height is $1.5D_{90}$, with particle properties in **Table 1**.

3. Wear phenomenon of blade spreader in experiment

Before the simulation of the spreading dynamics, the wear phenomenon of blade spreader is observed by the experiment. The spreading system mainly consists of a controlling system, a blade with thickness of 1 mm, baseplate, and worktop, as shown in **Fig. 3(a)**. The spreading speed of the blade is controlled by a servo motor, while the gap height between the baseplate and blade is controlled by inserting a series of feeler gauge into the gap, where the minimum thickness of feeler gauge is 10 μm . After feeding the powder onto the front of the blade through a vibrating feeder, the blade begins to spread the powder onto the baseplate. Before next experimental test, the gap height is patiently re-adjusted again, and the baseplate is carefully cleaned by a rush and a vacuum cleaner. By repeating a number of experiments, the bottom surface of the blade is scanned by a laser spectroscopy confocal microscopy (Kathmatic Inc, China).

In the experiment, the 53–106 μm stainless steel powder with number-based $D_{90} = 103 \mu\text{m}$ is used. Correspondingly, the gap height is enlarged to 150 μm . Although this kind of powder is larger than the ones used in simulation, the relative ratio of the gap height to particle diameter D_{90} is similar, i.e. $\delta/D_{90} = 1.46$ in the experiment while δ/D_{90}

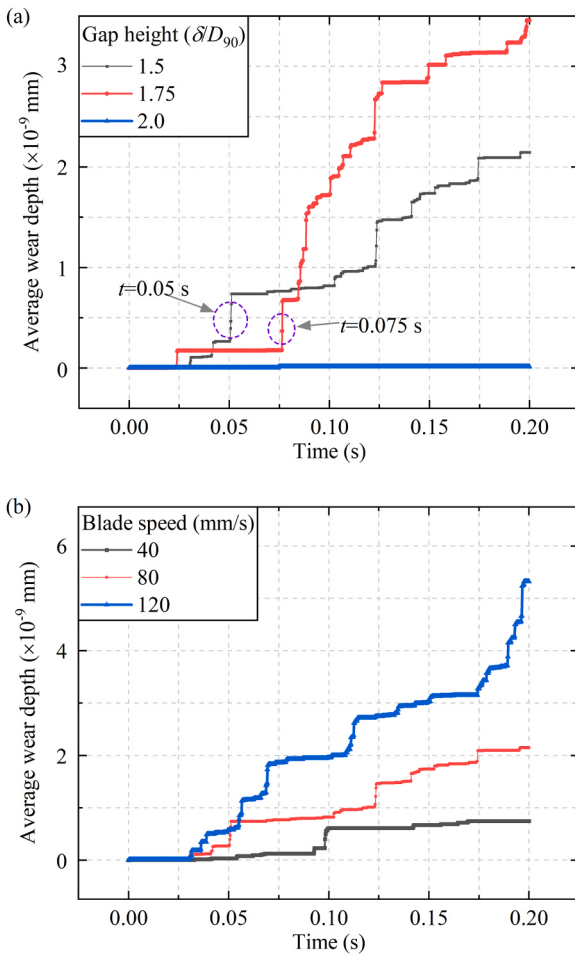


Fig. 4. Variation of average wear depth of blade with time at different (a) gap heights and (b) spreading speeds.

= 1.50 in the standard case in the simulation. In this way, the deviation of the gap height from the pre-set value is minimised, as the gap height with 150 μm is more easily to be adjusted and controlled than that with 67.5 μm . The spectrograms of the bottom surface of the blade are shown in Fig. 3(b), where 100 repetitive tests of powder spreading are carried out to observe the wear phenomenon of blade spreader. Dark red colour represents the highest point of the surface, while dark blue colour represents the lowest point of the surface. By comparing the spectrograms of the blade before spreading and after spreading, it could be found that the right region of the blade is topmost before spreading and it is worn to be the lowest region after spreading. It indicates that there is obvious wear at the bottom of the blade near the powder heap.

4. Results

4.1. Effect of the spreading conditions

In this section, the effect of spreading conditions on the wear of the blade spreader is studied, including gap height and spreading speed. For case S1, three kinds of gap heights are used: $\delta/D_{90} = 1.5, 1.75$ and 2.0 , while the spreading speed is the same as the standard case, i.e. $U = 80$ mm/s. For case S2, three kinds of spreading speeds are adopted: $U = 40$ mm/s, 80 mm/s and 120 mm/s, while the gap height is the same as the standard case, i.e. $\delta/D_{90} = 1.5$. In all cases, the particle properties are the same, as shown in Table 1.

Fig. 4 shows the variation of the average wear depth of the blade with time, where the average is done for all surfaces of the blade. The wear depth increases dramatically at several time points while changes

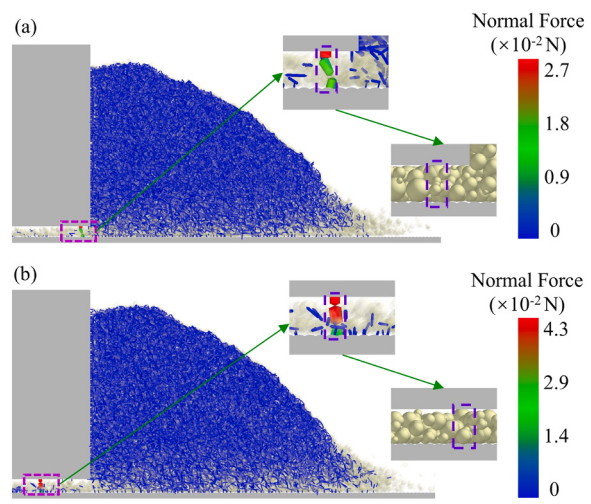


Fig. 5. Force chain and jammed particles for (a) $\delta/D_{90} = 1.5$ at 0.05 s and (b) $\delta/D_{90} = 1.75$ at 0.075 s.

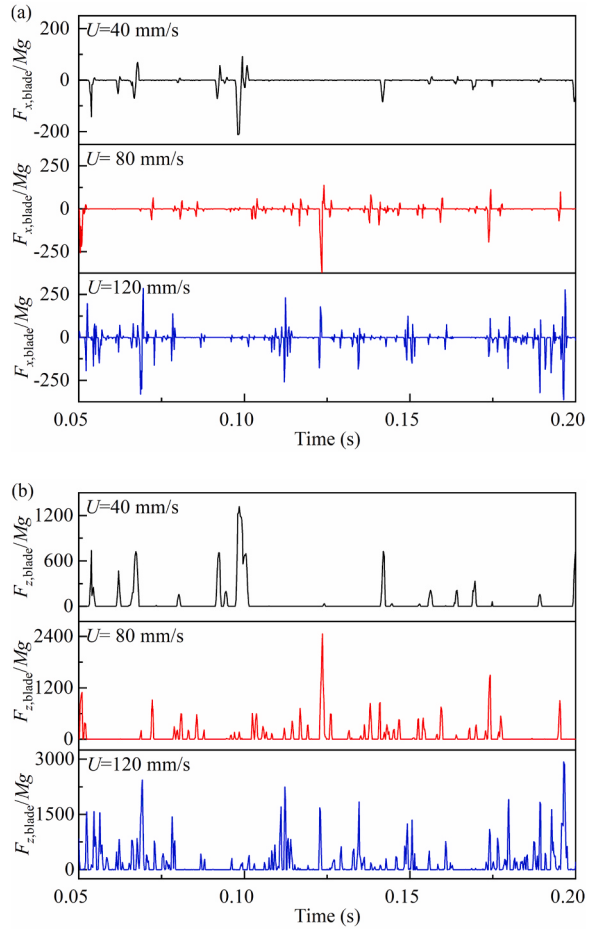


Fig. 6. Variation of total force on the blade with time at different spreading speeds: (a) force in the spreading direction; (b) force in the vertical direction.

little at other time points, which is in a stepwise style. The wear depth is significantly affected by the gap height and spreading speed. As shown in Fig. 4(a), the wear of the blade could be observed at $\delta/D_{90} = 1.5$ and $\delta/D_{90} = 1.75$, while the wear almost disappears when the gap height increases to $\delta/D_{90} = 2.0$. These results indicate that the wear of the blade is not due to the conventional interaction between the blade and

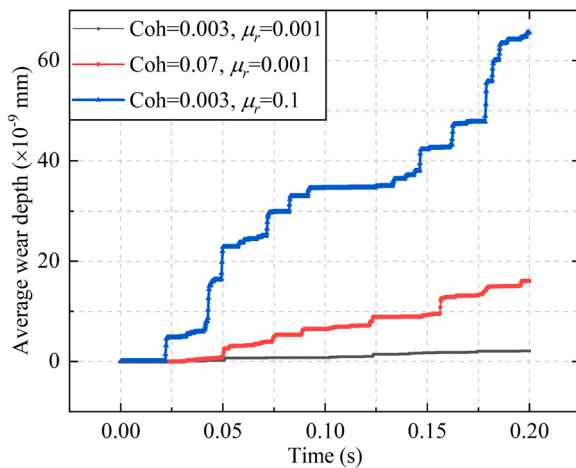


Fig. 7. Variation of average wear depth of blade with time in the cases with different particle properties.

bulk particle flow, otherwise, the wear depth would increase continuously with time for all gap heights. In reality, the wear of the blade is mainly due to particle jamming which occurs transiently at narrow gap, i.e. the gap is locally blocked by the particles, but the blade continues to move forward and finally break the jamming state, resulting in repetitive formation and disappearance of jamming. Here, two special time points are examined, i.e. $t = 0.05$ s for $\delta/D_{90} = 1.5$ at and $t = 0.075$ s for $\delta/D_{90} = 1.75$, where the wear depth is suddenly increased, as labelled in Fig. 4. The corresponding force chains at these two time points are shown in Fig. 5, which is coloured by the normal force. The snapshots of the particles are also embedded. A strong force chain could be observed at the gap between the base and blade bottom, and two particles are found to be jammed in the gap, validating the occurrence of jamming. The normal force of the jammed particles could even be 10,000 times of that of the un-jammed particles in the heap. As shown in Fig. 4(a), compared to the case of $\delta/D_{90} = 1.5$, the wear depth at $\delta/D_{90} = 1.75$ is larger. This is mainly due to stronger jamming at $\delta/D_{90} = 1.75$, which may need further investigation in future.

As shown in Fig. 4(b), the wear depth increases with the increase of spreading speed. For example, the wear depth increases almost 6 times as the spreading speed changes from 40 mm/s to 120 mm/s. Correspondingly, the variation of the total force on the blade $F_{x,\text{blade}}$ in the spreading direction and $F_{z,\text{blade}}$ in the vertical direction with time is shown in Fig. 6, where the force is normalised by the total weight of

powder heap Mg in front of the blade. According to above analysis, the large peaks of the force could be deemed as the occurrence of jamming. For the case with the spreading speed of 80 mm/s, the wear depth suddenly increases at $t = 0.125$ s, while there is a very large peak of the blade force at the same time point. It validates again that the wear is mainly due to particle jamming in the spreading gap. With the increase of spreading speed, both the strength and frequency of particle jamming increase, as indicated by the value of force at peaks and the number of peaks, resulting in larger wear depth. Meanwhile, for the case of the spreading speed of 120 mm/s, the wear depth almost increases continuously with time at 0.175–0.2 s. This is due to that the frequency of particle jamming is very high at this period as indicated by the peaks. These results show that the characteristics of the wear of the blade spreader are strongly related to the dynamic behaviour of particle jamming occurred in the spreading gap.

4.2. Effect of the particle properties

In this section, the effect of particle properties on the wear of blade spreader is studied, including interfacial surface energy Γ and rolling friction coefficient μ_r . For the former, cohesion number Coh is used to describe its effect on particle dynamics [10]:

$$Coh = \frac{\Gamma^{5/3}}{\rho g E^{2/3} R^{8/3}} \quad (10)$$

where $R^* = D_{90}/4$ is the equivalent radius between two identical particles with diameter of D_{90} . For the latter, it could partially indicate the effects of particle shape or particle interlocking on spreading dynamics. Here, three cases are compared: a) standard case, i.e. $Coh = 0.003$ and $\mu_r = 0.001$; b) more cohesive particle, i.e. $Coh = 0.07$ while μ_r is the same as the standard case; c) more stronger interlocking, i.e. $\mu_r = 0.1$ while Coh is the same as the standard case. In all cases, the spreading speed is $U = 80$ mm/s and the gap height is $\delta/D_{90} = 1.5$.

Fig. 7 shows the variation of the wear depth of the blade with time in different cases, which is averaged for all surfaces of the blade. Compared to the standard case (i.e. $Coh = 0.003$ and $\mu_r = 0.001$), the wear depth is increased by the increase of the cohesion number or rolling friction. The extent of the increase of the wear depth due to rolling friction is larger than that of cohesion number, indicating that the wear of the blade is more sensitive to the particle interlocking than particle cohesion. For example, at the time of 0.2 s, compared to the standard case, the average wear depth increases about 30 times as the rolling friction increases to 0.1, and about 6 times as the Coh increases to 0.07. The force chain coloured by the normal force is shown in Fig. 8, where only the time

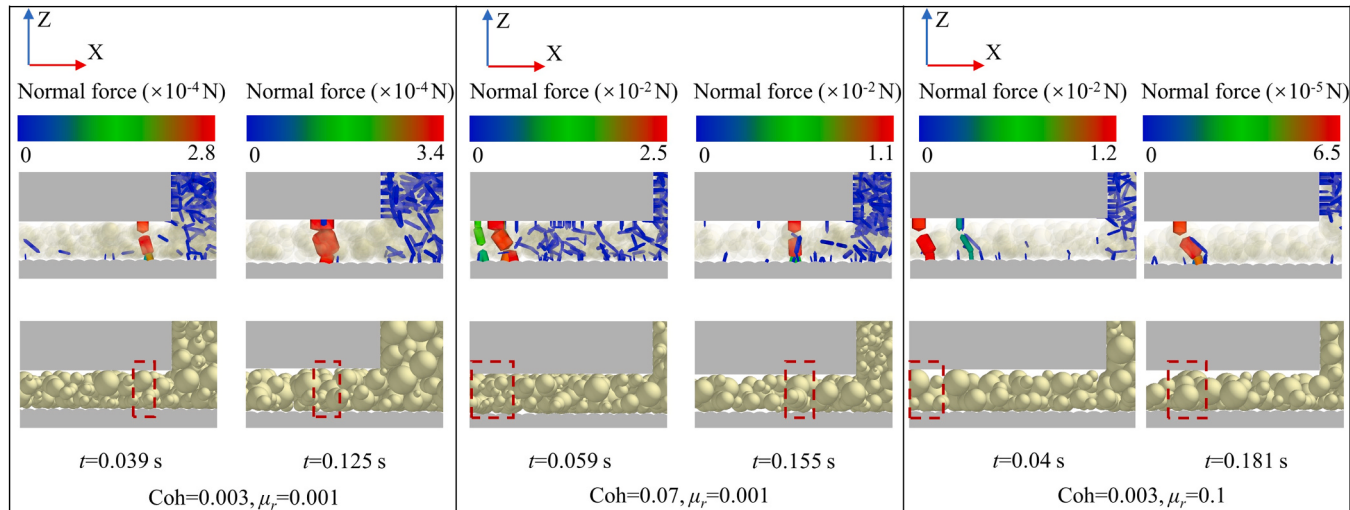


Fig. 8. Force chain and jammed particles in the cases with different particle properties.

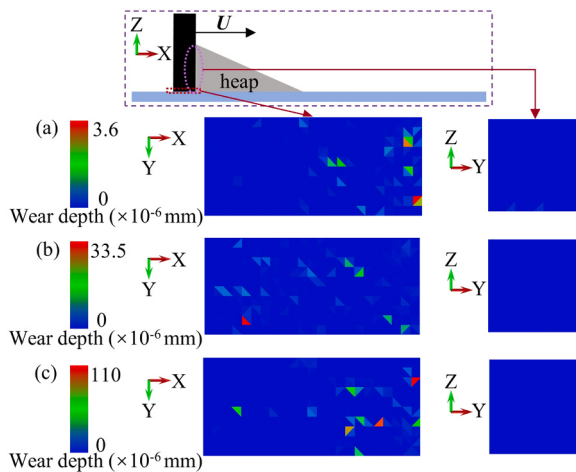


Fig. 9. Distribution of the wear depth on the bottom surface (left) and the front surface (right) of the blade at $t = 0.2$ s: (a) standard case ($Coh = 0.003, \mu_r = 0.001$); (b) $Coh = 0.07, \mu_r = 0.001$; (c) $Coh = 0.003, \mu_r = 0.1$.

point with a sudden increase of the wear depth is included. A strong force chain appears in the spreading gap, especially for the case with $Coh = 0.07$. It indicates again that the sudden increase of the wear depth is related to the occurrence of particle jamming. It should be noted that although the jamming in the case with $\mu_r = 0.1$ is weaker than that with $Coh = 0.07$, the wear depth with $\mu_r = 0.1$ is larger than that of $Coh = 0.07$, as shown in Fig. 7. It is mainly due to that the rolling friction could inhibit the relative rolling of the particles against the wall, promoting the sliding along the spreading direction, and thus resulting in a stronger wear, as shown in Eq. (6).

The local distribution of the wear depth of the blade is shown in Fig. 9. Both the bottom surface and the front surface (i.e. the surface in contact with the major heap) of the blade are included. It could be found that compared to the bottom surface, the wear depth at the front surface could be ignored. This is mainly due to that the wear in the front surface is mainly due to the conventional contact between particles and the front wall of the blade, while the wear in the bottom surface is mainly due to the transient jamming occurring within the gap. Of course, the wear of the blade could be ignored if there is no jamming anymore. With the increase of cohesion number or rolling friction, the maximum wear depth is much increased. For example, the maximum wear depth increases about 30 times as the rolling friction increases from 0.001 to 0.1. Fig. 9 also shows that the wear of the blade mainly occurs on bottom surface with locations close to the front tip of the blade.

4.3. Effect of the bumps on the base

In this section, three cases are used to study the influence of the bumps on the wear of the blade spreader: a) for case B1, three small and spherical bumps are uniformly distributed on the base; b) for case B2, bumps are made of clumped spheres; c) for case B3, three cylindrical bumps are used, which corresponds to the long and small bumps in the real actual AM process. In each case, three bumps are distributed at 4 mm, 8 mm and 12 mm on the base along the spreading direction, as shown in Fig. 10, with the time of 0.065 s, 0.115 s and 0.165 s for the blade reaching the centre of these bumps, respectively.

Fig. 11 shows the increment of the average wear depth of the blade during the spreading process. The period between the blade reaching and leaving the edges of the bump is indicated by a box with dotted line. There are large peaks at several time points, while the increment is almost zero at other time points, indicating that the wear depth increases with time in a stepwise style. Compared to the standard case, the magnitude of the peaks in case B1 and case B2 do not show much difference, even when the blade passes the bumps. For example, in case B1, the peak is about 0.2×10^{-9} mm around the second bump, but similar peaks could also be observed at several time steps in the standard case. It is interesting that peaks could be found in all regions with bumps in case B2, indicating that the bump could locally promote the occurrence of the jamming, and thus the wear of the blade. Especially, in the region around first bump, there are two large and adjacent peaks, which could not be observed in the standard case and case B1.

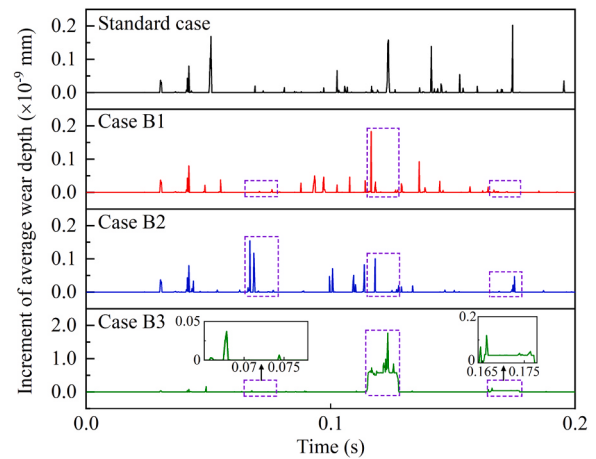


Fig. 11. Increment of average wear depth in different cases, where the period between the blade reaching and leaving the edges of the bump is indicated by a box with dotted line.

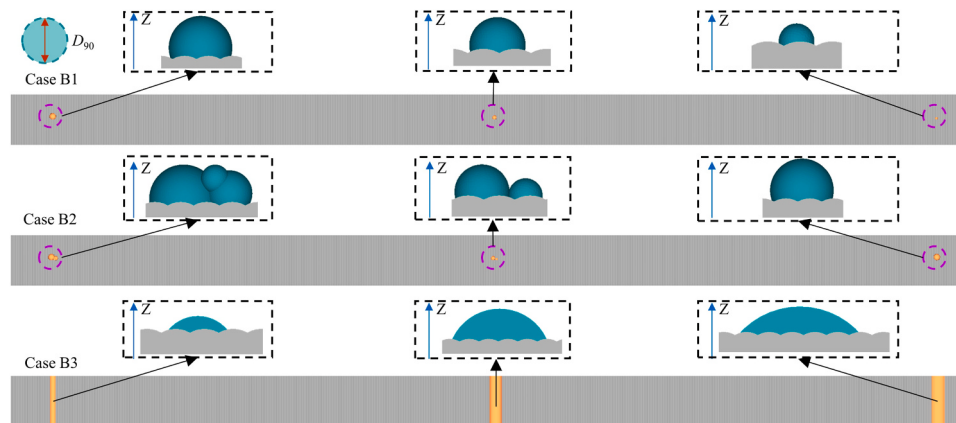


Fig. 10. Positions and shapes of the bumps on the base.

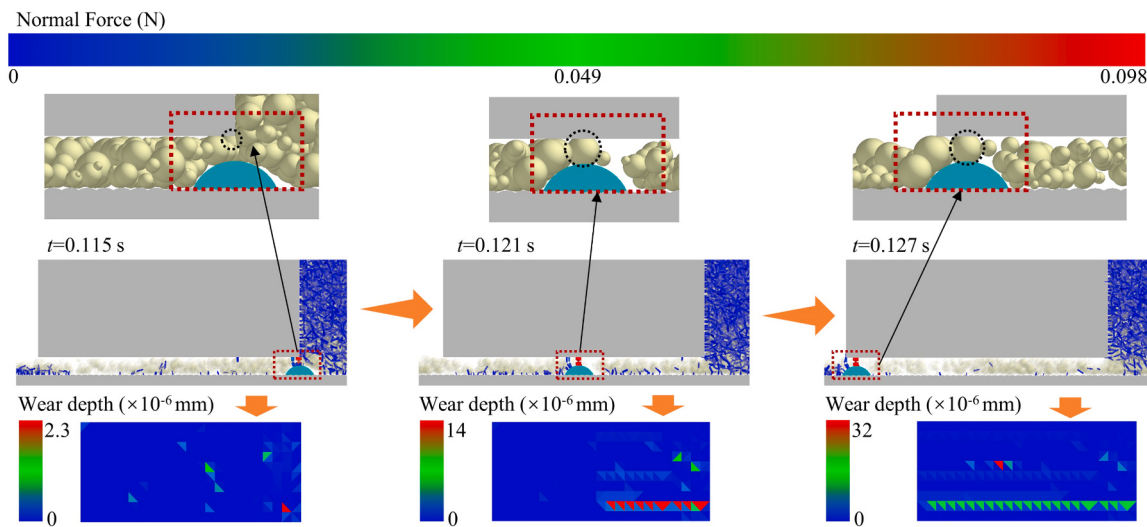


Fig. 12. Force chain and jammed particles in case B3, where the long scratch on the bottom surface of the blade is also included.

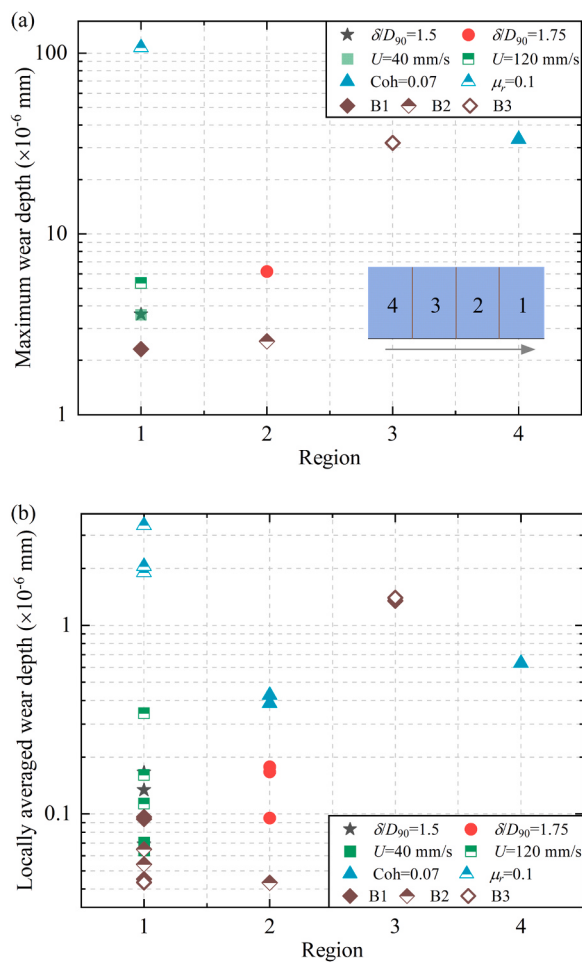


Fig. 13. Position of the maximum wear depth on the bottom surface of the blade: (a) maximum value of the whole surface at $t = 0.2$ s; (b) maximum value of the locally averaged depth among the 4 regions at $t = 0.1$ s, 0.15 s, 0.2 s.

In case B3, when the blade passes the second bump, i.e. the largest bump in this work, the peak of increment is much larger than that of other cases, i.e. about 10 times of the maximum value in case B1 and case B2. It is interesting that this increment could be kept for a long time.

As the peak of the increment also corresponds to the occurrence of the jamming, it may indicate that the jammed state of the particles is kept for a long time. Here, the snapshot of the particles and corresponding force chain are shown in Fig. 12. It could be found that a strong force chain forms when the blade reaches the bump, and it exists for a long period until the blade leaves the bump. The jammed particles almost slide against blade bottom during this period. Under this effect, there is a long scratch on the bottom surface of the blade.

5. Discussions

To identify the location where the wear could mostly occur, the bottom surface of the blade is divided into 4 regions along the spreading direction. The location of the maximum wear depth of the whole bottom surface is examined at 0.2 s, as shown in Fig. 13(a). The averaged wear depth of each region is calculated at 0.1 s, 0.15 s and 0.2 s, and the region with maximum value is examined, as shown in Fig. 13(b). It could be found that the wear is mainly in region 1, and then region 2. This is consistent with the wear phenomenon observed in the experiment. Meanwhile, the wear depth is sensitive to the rolling friction of particles, i.e. particle interlocking or particle shape. For example, as shown in Fig. 13(a), the maximum wear depth at $\mu_r = 0.1$ is about 30 times of that of the standard case. Fig. 13 also shows that the maximum wear depth is sensitive to the large bump on the base (i.e. the spatter formed in the sintering process of previous spread layer). The maximum value in Fig. 13(a) is about 30 times of that in Fig. 13(b), indicating that the distribution of wear is very un-uniform. This is consistent with the nature of jamming reported in this work, i.e. transient and random in space.

Fig. 13(a) shows that for most cases, the maximum wear depth is less than 10×10^{-3} μm . This is much smaller than the ones in the experiment, i.e. around 100 μm after 100 experimental tests for the same sample. It may be caused by several reasons: 1) Young's modulus is scaled down in the contact law of DEM to speed up the simulation, but when calculating the wear depth using Eq. (6), the hardness is kept at the same value as the ones without scaling; 2) the gap in the experiment maybe not well controlled due to the flatness of the baseplate, which is also worn by transient jamming; meanwhile, the baseplate becomes more and more rough, which promotes the jamming, and thus the wear is enlarged; 3) the simulation scale, such as the number of particles and system size, is much smaller than the ones in the experiment. More detailed reasons may need further investigation in future.

According to the position of wear shown in Fig. 13, and the mechanism of wear analysed in Section 4, a simple method is proposed here to

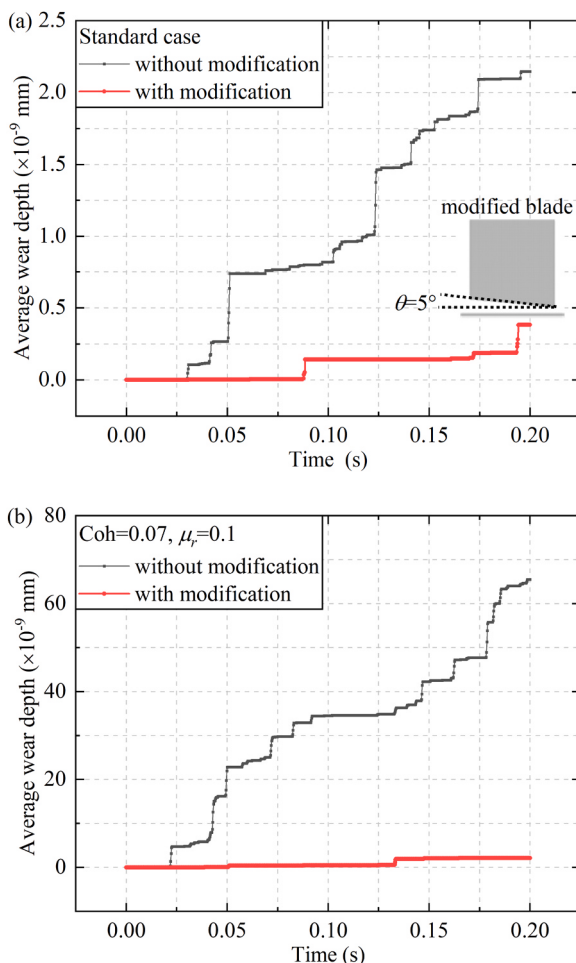


Fig. 14. Comparisons of the average wear depth between the conventional and modified blades: (a) standard case ($Coh = 0.003$, $\mu_r = 0.001$); (b) case with $Coh = 0.003$, $\mu_r = 0.1$.

reduce the wear of the blade: a rake angle of $\theta = 5^\circ$ is adopted at the bottom of the blade. Here, the standard case and the case with $\mu_r = 0.1$ are examined. The comparison of the average wear depth between the conventional blade and the modified blade is shown in Fig. 14. It could be found that the wear depth of the blade is much reduced after modification. For example, at the time point of 0.2 s in the case with $\mu_r = 0.1$, the wear depth of the modified blade could be reduced to about 3% of that of the conventional blade.

6. Conclusions

In this work, the wear of the blade spreader in the powder spreading process in Additive Manufacturing is studied. The wear phenomenon is firstly observed in the experiment, and then investigated by numerical simulation using Discrete Element Method, where the effects of spreading conditions, particle properties and the bumps on the base formed in the sintering process are considered. Main results from this work are summarised as follows:

- 1) A new mechanism for the wear of blade spreader is identified, i.e. transient jamming of particles. The characteristics of the wear are strongly related to the dynamic behaviour of particle jamming occurred in the gap between the spreader and base.
- 2) Significant wear of the blade spreader could be observed when the spreading gap is less than 2 times of particle diameter D_{90} , beyond which the wear could be avoided. The wear depth of the blade

spreader increases with time in a stepwise style, in which the sudden increase of the wear depth is related to the occurrence of jamming.

- 3) Larger wear depth could be induced by the increase of powder spreading speed, particle cohesion and particle interlocking. The bump or spatter on the base could locally promote the occurrence of the jamming, and thus the wear of the blade spreader, even resulting in a long scratch on the bottom of the blade spreader.
- 4) The wear mainly occurs at the bottom surface of the blade spreader, with locations close to the blade front tip. The maximum wear depth is sensitive to particle interlocking. A simple method is proposed to reduce the wear, i.e. using a rake angle to modify the bottom of the blade spreader.

CRediT authorship contribution statement

Lanzhou Ge: Investigation, Writing – original draft. **Rui Xu:** Investigation, Writing – original draft. **Wenguang Nan:** Conceptualization, Investigation, Writing – original draft, Writing – review & editing.

Declaration of Competing Interest

The authors declare that they have no known competing financial interests or personal relationships that could have appeared to influence the work reported in this paper.

Data Availability

Data will be made available on request.

Acknowledgments

The authors are grateful to the National Natural Science Foundation of China (Grant No. U2241248, 51806099, 32272358), National Key R&D Program of China (Grant No. 2022YFB4602200). The first author is also grateful to Postgraduate Research & Practice Innovation Program of Jiangsu Province (Project No. 1440). The corresponding author is also thankful to Professor Mojtaba Ghadiri, University of Leeds, UK, for the inspiration on this work.

References

- [1] Frazier WE. Metal additive manufacturing: a review. *J Mater Eng Perform* 2014;23: 1917–28.
- [2] Guo N, Leu MC. Additive manufacturing: technology, applications and research needs. *Front Mech Eng* 2013;8:215–43.
- [3] Herzog D, Seyda V, Wycisk E, Emmelmann C. Additive manufacturing of metals. *Acta Mater* 2016;117:371–92.
- [4] Macédo G, Pelcastre L, Hardell J. High temperature friction and wear of post-machined additively manufactured tool steel during sliding against AlSi-coated boron steel. *Wear* 2023;523.
- [5] Lizzul L, Sorgato M, Bertolini R, Ghiotti A, Bruschi S. Influence of additive manufacturing-induced anisotropy on tool wear in end milling of Ti6Al4V. *Tribology Int* 2020;146.
- [6] Haeri S, Wang Y, Ghita O, Sun J. Discrete element simulation and experimental study of powder spreading process in additive manufacturing. *Powder Technol* 2017;306:45–54.
- [7] Nan W, Pasha M, Bonakdar T, Lopez A, Zafar U, Nadimi S, et al. Jamming during particle spreading in additive manufacturing. *Powder Technol* 2018;338:253–62.
- [8] Shaheen MY, Thornton AR, Luding S, Weinhardt T. The influence of material and process parameters on powder spreading in additive manufacturing. *Powder Technol* 2021;383:564–83.
- [9] Yim S, Bian H, Aoyagi K, Yamanaka K, Chiba A. Spreading behavior of Ti 48Al 2Cr 2Nb powders in powder bed fusion additive manufacturing process: experimental and discrete element method study. *Addit Manuf* 2021;49.
- [10] Xu R, Nan W. Analysis of the metrics and mechanism of powder spreadability in powder-based additive manufacturing. *Addit Manuf* 2023;71.
- [11] Zolotarevskiy V, Corujeira Gallo S, Pereira MP, Barnett MR. Modelling of impeller-tumbler wear test with discrete element method. *Wear* 2022;510–1.
- [12] Thompson JA, Berry L, Southern S, Walls WK, Holmes MA, Brown SGR. The effect of mesh discretisation on damage and wear predictions using the Discrete Element Method. *Appl Math Model* 2022;105:690–710.
- [13] Katinas E, Chotěborský R, Linda M, Kuře J. Sensitivity analysis of the influence of particle dynamic friction, rolling resistance and volume/shear work ratio on wear

- loss and friction force using DEM model of dry sand rubber wheel test. *Tribology Int* 2021;156.
- [14] Leonard BD, Sadeghi F, Shinde S, Mittelbach M. Rough surface and damage mechanics wear modeling using the combined finite-discrete element method. *Wear* 2013;305:312–21.
- [15] Ilic D. Development of design criteria for reducing wear in iron ore transfer chutes. *Wear* 2019;434–5.
- [16] Rojas E, Vergara V, Soto R. Case study: discrete element modeling of wear in mining hoppers. *Wear*, 430- 2019;431:120–5.
- [17] Capozza R, Hanley KJ. A comprehensive model of plastic wear based on the discrete element method. *Powder Technol* 2022;410.
- [18] Phan HT, Tieu AK, Zhu H, Kosasih B, Zhu Q, Grima A, et al. A study of abrasive wear on high speed steel surface in hot rolling by Discrete Element Method. *Tribology Int* 2017;110:66–76.
- [19] Katinas E, Choteborský R, Linda M, Jankauskas V. Wear modelling of soil ripper tine in sand and sandy clay by discrete element method. *Biosyst Eng* 2019;188: 305–19.
- [20] Kalácska Á, De Baets P, Fauconnier D, Schramm F, Frerichs L, Sukumaran J. Abrasive wear behaviour of 27MnB5 steel used in agricultural tines. *Wear* 2020; 442–3.
- [21] Cundall PA, Strack ODL. A discrete numerical model for granular assemblies. *Geotechnique* 1979;29:47–65.
- [22] Thornton C. *Granular Dynamics, Contact Mechanics and Particle System Simulations*. New York: Springer; 2015.
- [23] Johnson KL, Kendall K, Roberts AD. Surface energy and the contact of elastic solids. *Proc. R. Soc. Lond. A Math Phys Sci* 1971;324:301–13.
- [24] Archard JF. Contact and rubbing of flat surfaces. *J Appl Phys* 1953;24:981–8.
- [25] Peterson MB, Winer WO. *Wear control handbook*; 1980.
- [26] Washino K, Chan EL, Tanaka T. DEM with attraction forces using reduced particle stiffness. *Powder Technol* 2018;325:202–8.
- [27] Haervig J, Kleinhans U, Wieland C, Spliethoff H, Jensen AL, Sørensen K, et al. On the adhesive JKR contact and rolling models for reduced particle stiffness discrete element simulations. *Powder Technol* 2017;319:472–82.
- [28] Nassar AR, Gundermann MA, Reutzel EW, Guerrier P, Krane MH, Weldon MJ. Formation processes for large ejecta and interactions with melt pool formation in powder bed fusion additive manufacturing. *Sci Rep* 2019;9:5038.
- [29] Ladewig A, Schlick G, Fisser M, Schulze V, Glatzel U. Influence of the shielding gas flow on the removal of process by-products in the selective laser melting process. *Addit Manuf* 2016;10:1–9.
- [30] Young ZA, Guo Q, Parab ND, Zhao C, Qu M, Escano LI, et al. Types of spatter and their features and formation mechanisms in laser powder bed fusion additive manufacturing process. *Addit Manuf* 2020;36.